RSC Advances

PAPER

View Article Online
View Journal | View Issue

Cite this: *RSC Adv.*, 2022, **12**, 11708

Cell penetrating peptide decorated magnetic porous silicon nanorods for glioblastoma therapy and imaging†

Arnaud Chaix, ‡[a] Audrey Griveau,‡[b] Thomas Defforge,[a] Virginie Grimal,[a] Brice Le Borgne,[a] Gaël Gautier*[a] and Joël Eyer*[b]

Glioblastoma multiforme (GBM) is the most malignant primary brain tumor of the central nervous system. Despite advances in therapy, it remains largely untreatable, in part due to the low permeability of chemotherapeutic drugs across the blood–brain barrier (BBB) which significantly compromises their effectiveness. To circumvent the lack of drug efficiency, we designed multifunctional nanoparticles based on porous silicon. Herein, we propose an innovative synthesis technique for porous silicon nanorods (pSiNRs) with three-dimensional (3D) shape-controlled nanostructure. In order to achieve an efficient administration and improved treatment against GBM cells, a porous silicon nanoplatform is designed with magnetic guidance, fluorescence tracking and a cell-penetrating peptide (CPP). A NeuroFilament Light (NFL) subunit derived 24 amino acid tubulin binding site peptide called NFL-TBS.40-63 peptide or NFL-peptide was reported to preferentially target human GBM cells compared to healthy cells. Motivated by this approach, we investigated the use of magnetic-pSiNRs covered with superparamagnetic iron oxide nanoparticles (SPIONs) for magnetic guidance, then decorated with the NFL-peptide to facilitate targeting and enhance internalization into human GBM cells. Unexpectedly, under confocal microscope imaging, the internalized multifunctional nanoparticles in GBM cells induce a remarkable exaltation of green fluorescence instead of the red native fluorescence from the dye due to a possible Förster resonance energy transfer (FRET). In addition, we showed that the uptake of NFL-peptide decorated magnetic-pSiNRs was preferential towards human GBM cells. This study presents the fabrication of magnetic-pSiNRs decorated with the NFL-peptide, which act as a remarkable candidate to treat brain tumors. This is supported by *in vitro* results and confocal imaging.

Received 24th January 2022
Accepted 30th March 2022

DOI: 10.1039/d2ra00508e

rsc.li/rsc-advances

Introduction

Glioblastoma multiforme (GBM) is extremely invasive and considered among the deadliest brain cancers.[1] GBM is a high-grade (grade IV) glioma according to the World Health Organization, and is fast growing, spreads within the brain and may come back even if extensively treated. In 2018, the National Institute of Health (NIH) predicted around 24 000 new cases of GBM brain cancer in the United States with a constant increase. Nowadays, the standard treatment required for GBM is surgical resection followed by radiotherapy and chemotherapy.[2] However, the recovery of patients with GBM is less than 5% over 5 years.[3] The persistent limitations for such treatments include their low specificity to the tumor, possibly causing irreversible side effects and the risk of developing resistance to the treatment.[4] Moreover, the delivery of drugs into the brain can be limited by the low permeability of the blood–brain barrier (BBB), which causes the inefficiency of conventional therapeutics such as chemotherapeutic drugs. There is a dire need to search for new GBM treatment strategies and nowadays nanomedicine appears as one of the most promising approaches.

During the past few decades, nanomedicine has emerged as an alternative strategy to overcome the limitation mentioned above and address effective anti-cancer treatments.[5] However, to improve the GBM treatment, the development of new therapeutic platforms such as functionalized nanoparticles (NPs) has become crucial to cross the BBB, reach the brain tumor and release an optimal dose of drugs. Interestingly, the development of those targeting NPs for drug delivery have certain advantages such as the prevention of premature release or drug degradation or an increased cellular uptake. In fact, a wide range of nanoparticles have been developed and studied as anticancer therapeutics against GBM cells including lipidic nanocapsules,[6,7] polymeric NPs,[8,9] mesoporous silica nanoparticles

[a]GREMAN UMR-CNRS 7347, INSA Centre Val de Loire, Université de Tours, Tours, France. E-mail: gael.gautier@univ-tours.fr

[b]MINT, INSERM, CNRS, SFR-ICAT, UNIV Angers, 49000 Angers, France. E-mail: joel.eyer@univ-angers.fr

† Electronic supplementary information (ESI) available. See https://doi.org/10.1039/d2ra00508e

‡ These authors contributed equally.

(MSN),[10,11] and Metal–Organic Frameworks (MOFs) NPs.[12,13] Among these materials, porous silicon nanoparticles (pSiNPs) are being considered as especially promising owing to their physico-chemical properties, biocompatibility, biodegradability and the low toxicity of the degradation by-products *in vivo*.[14] In particular, orthosilicate, which is non-toxic and inert for human cells, is the major degradation by-product of pSi.[15] Besides, silicon is an oligo-element naturally present in significant amount in the human tissues, whether bone, organic or connective. One of the main advantages of pSi materials compared to other nanomaterials is the possibility of accurately adjusting the structures, shapes, porosity, and pore size according to the intended application. For instance, pSi materials can exhibit high specific surface area (up to 1125 $m^2 g^{-1}$), high porosity (in the 30–95% range) and large pores size.[16–18] These morphological properties combined with the silicon surface chemistry enable versatile surface modification opportunities and therefore a large range of targeting ligand functionalizations such as peptides,[7,19] antibodies,[20,21] sugars,[22,23] and molecules.[24] Moreover, pSiNPs have been extensively investigated for drug encapsulation with an exceptional loading capacity[25] and a variety of therapeutic drugs for instance chemotherapeutics,[26,27] oligonucleotides,[19] and nucleic acid.[28,29] To our knowledge some studies have already been reported using pSiNPs as a nanoplatform for targeting and therapy of GBM.[30–33] Subsequently, composite nanomaterials based on pSiNPs have been also reported for biological applications in particular with the decoration with smaller size nanoparticles typically gold nanoparticles NPs,[34] silver NPs,[35] and superparamagnetic iron oxide NPs (SPIONs).[27] To this aim, we focused our effort on novelties including (3D) shape-controlled nanostructure fabrication of pSi and multiple functionalities of the nanoplatform such as magnetic guidance, fluorescent tracking, and cell-penetrating peptide (CPP) carrying, the latter leading to GBM cellular death. Then, SPIONs were used to decorate the fabricated nanorods and appear as a useful strategy to reach the human GBM cells by transportation under magnetic field. Specifically, SPIONs already demonstrated to be a powerful nanomaterial for biological applications due to their low-toxicity,[36–38] Magnetic Resonance Imaging (MRI) contrast agent[39,40] efficiency and their magnetic field guidance ability.[27] In addition, fluorescent dye (DiD, see ESI†) was loaded into the mesoporous structure of pSiNRs for fluorescent tracking under confocal microscope imaging. In this study, a peptide corresponding to the sequence of the NeuroFilament Light subunit which binds tubulin (NFL-TBS.40-63 peptide for NeuroFilament Low Subunit-Tubulin Binding Site 40-63), also called NFL-peptide was used. This peptide interacts or penetrates specifically in all glioblastoma cell lines tested (rat, mouse, human and dog), and by blocking the polymerization of microtubules, it inhibits cell division *in vitro* and *in vivo*.[41,42] To date, some studies report the used of NFL-peptide as targeting agent and Eyer and co-workers pioneering work led to the development of targeted-nanoparticles based on NFL-peptide.[38,43,44] Indeed, a recent study reported by Karim *et al.* demonstrates the use of lipid nanocapsules decorated with NFL-peptide which were preferentially internalized into human, rat and mouse's GBM cells instead of healthy human cells.[7] To this mean, the physico-chemical properties of the functionalized nanoparticles were fully characterized and *in vitro* studies, cellular internalization of the nanoparticles by transmission electron microscopy (TEM) and confocal microscope imaging were performed.

Results and discussion

Preparation of porous silicon nanorods (pSiNRs)

pSiNPs size, shape, pore size and surface chemistry are of highest importance to the success of the study. Herein, we summarize the elaboration of pSiNRs controlled in shape and size using a two steps process. To this aim, pSiNRs were fabricated from an innovative way combining electrochemical etching[14] of silicon wafer followed by Metal-assisted Chemical Etching (MaCE)[45,46] obtaining a nanorod shape depicted in Fig. 1. This fabrication technique takes its origin to the need of the synthesis of particles with homogeneous dimensions in 3D over the single direction pSiNPs that we actually find in most of the scientific literature.[47,48] First, pSi was fabricated by electrochemical etching of boron doped p type silicon wafer in an electrolytic solution of deionized water, acetic acid, and hydrofluoric acid (5% HF). During the electrochemical etching leading to pSi formation, periodic "perforations" were carried out alternating "low" and "high" current density periods (for detailed information: see the ESI†). Hence, porous layers with alternating low and high porosity strata in depth were obtained with a periodicity of 200 nm. Scanning electron microscopy (SEM) confirmed the observation of this stratified layers (Fig. S1, ESI†). Thereafter perforated pSi layer was subjected to MaCE treatment in presence of HF and Ag^+ ions in order to fabricate perforated porous silicon nanowires (pSiNWs) (Fig. S2, ESI†). The Fig. S3 in the ESI† revealed the different steps of the preparation of the perforated pSiNWs on 6″ silicon wafers. The pSiNWs were then mechanically peeled off the parent substrate and dispersed into deionized (DI) water solution (Fig. S4, ESI†) and fractured by ultrasonication for 24 hours (Fig. S5, ESI†). During the ultrasonication step, the nanowires preferentially break at the level of the most fragile zone (the most porous) region of the strata therefore producing nanoparticles with repeatable dimensions. From this fabrication process, the nanoparticles were calibrated in the three directions: x direction (in the depth of the silicon wafer direction) during the electrochemical etching (stratified layer), and y and z directions during the MaCE leading to nanowires formation as described on the Fig. 1. After sonication and a series of centrifugation, a desired size of pSiNRs (between 250–500 nm) was obtained and characterized by TEM, SEM and dynamic light scattering (DLS). The SEM and TEM also validated the 3D controlled nanostructures, their monodispersity and mesoporosity with an average pore size of 10 to 15 nm (Fig. 2a, b, S6 and S7, ESI†). The apparent nitrogen adsorption and desorption measurements revealed the mesoporous structure of pSiNRs with a Brunauer–Emmett–Teller surface area (S_{BET}) of 293 $m^2 g^{-1}$ and a BJH (Barrett–Joyner–Halenda) desorption average pore diameter of 10 nm (Fig. S8a, ESI†). The pSiNRs display large pore volume and high specific surface area, suitable for grafting and loading

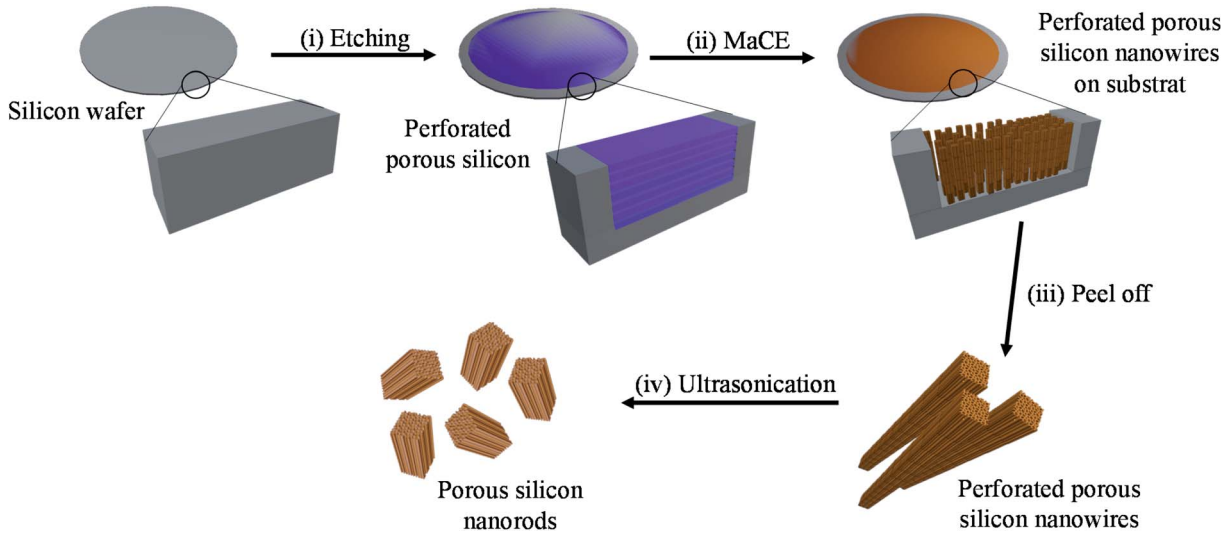

Fig. 1 Schematic representation of the preparation of porous silicon nanorods (pSiNRs): (i) etching, (ii) MaCE, (iii) peel off, and (iv) ultrasonication.

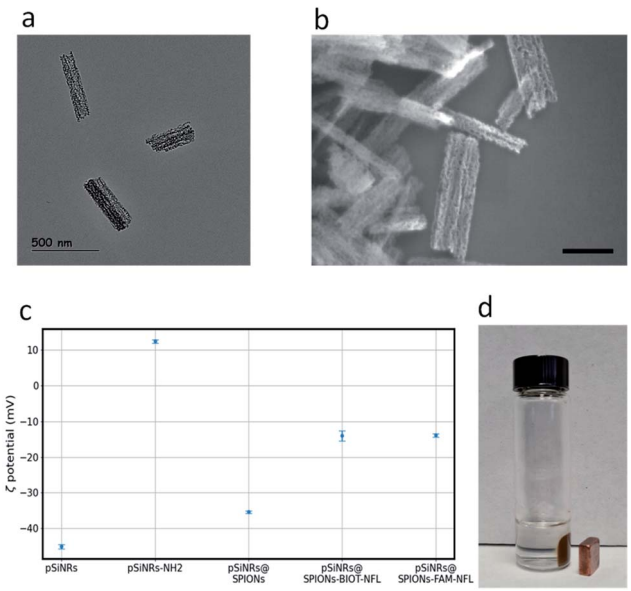

Fig. 2 (a) Transmission electron microscopy image of pSiNRs. Scale bar: 500 nm (b) scanning electron microscopy image of pSiNRs. Scale bar: 200 nm (c) ζ-potential measurements at each step of modifications. Bars represent mean ± SD ($n = 3$). (d) Photography of magnetic-pSiNRs under magnetic field.

of molecules. The (DLS) confirmed an average hydrodynamic diameter of pSiNRs at 250 nm with a polydispersity index of 0.17, which is in agreement with the observation of TEM and SEM images (Fig. S8b, ESI†). As expected, surface charge of the fresh pSiNRs was determined by zeta potential (ZP) measurement with negative value of −40 mV in deionized water (Fig. 2c). The negative charge value of the pSiNRs was ascribed to the surface oxidation during the MaCE. Additionally, powder X-ray diffraction (PXRD) confirmed the crystalline structure of the pSiNRs network (Fig. S8d, ESI†).

Preparation of the multifunctional nanoparticles

In this research project, pSi-based nanoplatforms against human GBM cells were designed. Eight different formulations were prepared to determine the influence of each new functionalization on GBM cell eradication. Those eight formations are designed as: fresh pSiNRs, the ones containing the fluorescent dye loaded into the mesoporous structure (pSiNRs-DiD), the ones containing SPIONs (pSiNRs@SPIONs, pSiNRs-DiD@SPIONs) and four with the BIOT-NFL-peptide [biotinylated] or with FAM-NFL-peptide [tag with fluorescein] (pSiNRs@SPIONs-BIOT-NFL, pSiNRs@SPIONs-FAM-NFL,

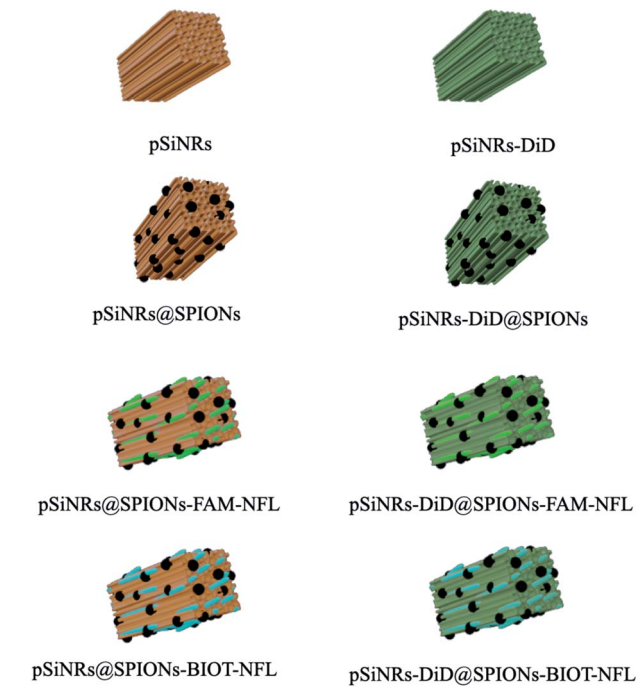

Fig. 3 Schematic representation of the nanoparticle formulations.

pSiNRs-DiD@SPIONs-BIOT-NFL, and pSiNRs-DiD@SPIONs-FAM-NFL) (Fig. 3).

The first step consists in grafting of (3-aminopropyl)triethoxysilane (APTES) onto fresh pSiNRs in ethanoic solution under reflux condition (Scheme S1, ESI†). The post chemical modification of fresh pSiNRs with an amine as a terminal group has been an obvious approach to provide a higher interaction with the negative charges of the SPIONs. Zeta potential and DLS measurements confirmed the attachment of the amine groups onto the surface *via* silanisation reaction (Fig. 2c and S9, ESI†). The DLS exhibits an increase of the hydrodynamic diameter from 250 nm to 381 nm (Fig. S9a, ESI†) attributed to a strong aggregation of the pSiNRs-NH_2 owed to the amine protonation in deionized water, which is in accordance with the literature.[29] After the chemical grafting of the APTES, the zeta potential value change from negative charge (−40.5 mV) to positive charge (+12 mV) (Fig. S9b, ESI†). ATR-FTIR spectroscopy was also performed with pSiNRs-NH_2 with the observation of the narrow band centered at 800 cm^{-1} ascribed to the amine function from the APTES moiety and an increase of surface oxidation compared to the fresh pSiNRs (Fig. S10, ESI†). The quantification of the attached APTES moiety was determined by thermogravimetric analysis (TGA) with a grafted amount of 0.014 mmol per mg of nanoparticles (Fig. S11, ESI†). To guide pSiNRs under magnetic field, 10–15 nm sized SPIONs (Fig. S12, ESI†) were attached to the particles (Scheme S2, ESI†). The magnetic-pSiNRs (pSiNRs@SPIONs) were harvested by centrifugation without need of magnetic washed attraction of the non-absorbed SPIONs, which showed high affinity between aminated-pSiNRs and SPIONs (Fig. S13, ESI†). The high amount of SPIONs decorated provide efficient transportation of the pSiNRs@SPIONs by using neodymium magnet (Fig. 2d and ESI†). The presence of pSiNRs@SPIONs was also characterized *via* several techniques. TEM and SEM confirmed the preferential self-assembly of the SPIONs onto the surface of pSiNRs-NH_2 and pointed out a homogeneous distribution (Fig. S14 and S15, ESI†). EDX analysis and mapping showed the presence of SPIONs onto the surface of the nanorods with the presence of the rays (Fe Lα, Fe Kα and Fe Kβ) and with approximatively 15% of iron element (Fig. S16 and S17, ESI†). DLS and ZP measurements gave additional indications on the dimensions and surface chemistry of pSiNRs@SPIONs (Fig. S18, ESI†). The hydrodynamic diameter of the formulations showed non-aggregated nanoparticles on contrary to pSiNRs-NH_2. This phenomenon can be explained by the negative charge value of the SPIONs attached the pSiNRs, which favors a higher solubility and dispersibility in deionized water. The crystal structure of pSiNRs@SPIONs was investigated by powder X-ray diffraction (PXRD) technique and displayed typical peaks that correspond to the SPIONs (Fig. S19, ESI†). As mentioned previously, in this research study, an additional functionality to the nanosystem has been added by the loading of fluorescent dye (DiD), which was realized on pSiNRs for pSiNRs-DiD (Scheme S3, ESI†) and simultaneously with the SPIONs for pSiNRs-DiD@SPIONs (Scheme S4, ESI†). Several characterizations techniques including DLS, ZP, FTIR, and UV-vis spectroscopy confirmed the successful loading of the DiD dye into the mesoporous structure of the nanorods (Fig. S20 and S22, ESI†). The ATR-FTIR presented new intense band appeared at 2875–2920 cm^{-1}, which corresponds to the stretching vibration of the C–H band (signature of the aliphatic chain of the DiD) (Fig. S21, ESI†). The UV-vis spectroscopy presented an absorption peak at 660 nm which corresponds to the absorbance pic of the DiD molecules (Fig. S22, ESI†). The presence of DiD dye into the framework of the nanoparticles allows us an optical tracking into the human GBM cells with the help of a confocal imaging microscope. Finally, CPP-magnetic-pSiNRs with or without fluorescent dye were prepared as described on the Schemes S5 and S6 (ESI†), along for enabling selective targeting and lead cellular death. The nanoparticles formulation was decorated with NFL-peptides (coupled with BIOT and FAM). Regarding the incorporation of CPP to the pSiNRs, we have privileged the decoration onto magnetic-pSiNRs instead of covalent bonding due to the loss of efficiency, which was previously demonstrated.[7] The presence of the NFL-peptide onto the surface of the magnetic-pSiNRs was also investigated by a complete characterization of the nanoparticles. The nanoparticles formulations containing the BIOT – or FAM-NFL-peptides onto the surface were also fully characterized by several techniques such as TEM, SEM, DLS and ZP (Fig. S23 and S27, ESI†). The DLS and ZP confirmed the successful decoration of the peptides with an increase in size diameter and surface charge of the formulations (Fig. S26 and S27, ESI†). This is further supported by ATR-FTIR characterizations with new intense band appeared at 2920–2875 cm^{-1}, assignable to the stretching vibration of the C–H band (aliphatic chain of the NFL-peptide and aliphatic chain of DiD). In addition, new peaks at 1525 cm^{-1} and 1625 cm^{-1} were observed, which are attributed to the functional groups of the NFL-peptide (amide and carboxylic acid groups) (Fig. S28 and S30, ESI†). The amount of BIOT-NFL-peptide decorated onto the magnetic-pSiNRs was determined by TGA analysis with a loading amount of 0.04 mmol of BIOT-NFL per mg of nanoparticles (Fig. S31, ESI†). In addition, a characteristic absorbance peak of fluorescein from FAM-NFL-peptide was observed at 490 nm by UV-vis spectroscopy (Fig. S32, ESI†). Therefore, these results suggest that the NFL-peptides were strongly absorbed to the surface of the nanoparticles. To conclude, the final nanoconstructs maintained their magnetic properties after the peptides modifications as showed on the Fig. S33 in the ESI.†

In vitro studies of the nanoparticles

The aim of this study was to evaluate and compare the effect on mitochondrial activity of the formulations. To evaluate the viability of F98 rat GBM cells, their mitochondrial activity was evaluated in presence of pSiNRs, pSiNRs@SPIONs, pSiNRs@SPIONs-BIOT-NFL, or pSiNRs@SPIONs-FAM-NFL at different concentrations (25, 50, 100 and 200 μg mL^{-1}) for 72 hours. Cells were also treated with 1 μg mL^{-1} of colchicine, used as a positive control, because colchicine interacts with tubulin and disrupts the assembly of microtubules.[49] In Fig. 4, MTS assay showed a strong decrease of F98 cells viability in presence of colchicine. However, no cellular toxicity of pSiNRs and

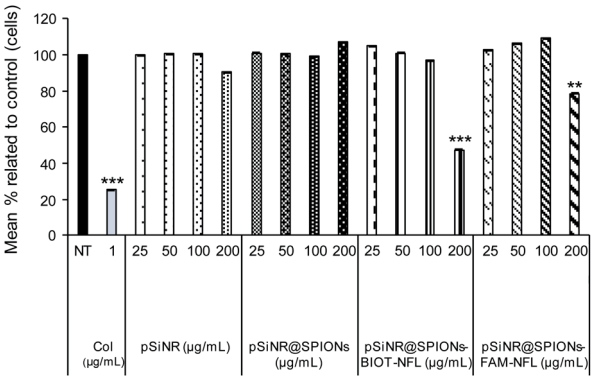

Fig. 4 *In vitro* effects of the pSiNRs without or with SPIONs, and without or with NFL-peptides (BIOT or FAM) on mitochondrial activity of rat glioblastoma cells (F98). Cells were treated with the formulations (25, 50, 100 or 200 μg mL^{-1}) or with the positive control colchicine (col, 1 μg mL^{-1}), for 72 hours, and mitochondrial activity was evaluated by MTS assay. Experiments were performed at least in triplicate. Data are represented as mean ± SEM. Statistical analysis was performed with Student's *t*-test (**$p < 0.005$ and ***$p < 0.001$).

pSiNRs@SPIONs, even at the highest concentrations, was observed. When the NFL-peptide (BIOT or FAM) was added on pSiNRs@SPIONs, a toxicity was observed with the highest concentration (200 μg mL^{-1}). The BIOT-NFL-peptide seems to be more effective than the FAM-NFL-peptide. The same experiments were carried out on neuroblastoma cells (SH-SY5Y), and no effect on mitochondrial activity was observed (Fig. S34, ESI†). These results demonstrate that the NFL-peptide retains its biological activity on GBM cells.

Cellular internalization of nanoparticles by transmission electronic microscopy

In the study, we evaluated the capacity of pSiNRs@SPIONs coupled or not with the NFL-peptide (BIOT or FAM) to be internalized in GBM cells. F98 cells were treated with pSiNRs@SPIONS, pSiNRs@SPIONs-BIOT-NFL, or pSiNRs@SPIONs-FAM-NFL at 200 μg mL^{-1} for 72 hours. After fixation and inclusion in the resin, cells were sectioned and observed with a TEM. A treatment with pSiNRs@SPIONs showed some nanoparticles are present in cells (Fig. 5a). When the NFL-peptide are added to pSiNRs@SPIONs, the cellular morphology changed, cells present more vacuoles (V), and more nanoparticles are detected in the GBM cells (Fig. 5b and c). No difference is observed between pSiNRs@SPIONs-BIOT-NFL (Fig. 5b) and pSiNRs@SPIONs-FAM-NFL (Fig. 5c). The presence of pSiNRs@SPIONs does not affect the biological activity of the NFL-peptide.

Cellular internalization of nanoparticles by confocal microscopy

To evaluate the cellular internalization of the nanoparticles, cells were treated with formulations loaded with DiD and the images were taken with confocal microscope. Four formulations (pSiNRs-DiD, pSiNRs-DiD@SPIONs, pSiNRs-DiD@SPIONs-BIOT-NFL, and pSiNRs-DiD@SPIONs-FAM-NFL) at 10 μg mL^{-1} were tested on F98 cells for 24 hours. The concentration of 10 μg mL^{-1} was chosen for confocal experiment to prevent any signal saturation of DiD. Orthogonal projections obtained with confocal microscope images are presented in the Fig. 6. In the Fig. 6, we observed a DiD fluorescence in the GBM cells with all conditions demonstrating an internalization of the nanoparticles in F98 cells. An important variation of DiD fluorescence was observed, even though the cells were treated under the same protocol. When F98 cells are treated with pSiNRs-DiD, some cells do not show DiD fluorescence. When SPIONs are added to the pSiNRs, the DiD fluorescence is stronger (Fig. 6) and more surprisingly a green fluorescence appears (Fig. S35†).

The addition of the NFL-peptide to the pSiNRs-DiD increase the DiD fluorescence. The confocal observations have demonstrated the capacity of pSiNRs-DiD@SPIONs with the NFL-peptides (BIOT or FAM) to internalize in the GBM cells. However, the presence of SPIONs combined with pSiNRs induced a green and a red fluorescence. As the green fluorescence appears when the SPIONs are added, to go further, another type of nanoparticles was tested: lipid nanocapsules (LNC) loaded with DiD, without and with SPIONs (LNC-DiD-SPIONs). Rat GBM cells were treated with LNC-DiD or with LNC-DiD-SPIONs at 2 mg mL^{-1} for 24 hours, then cells were

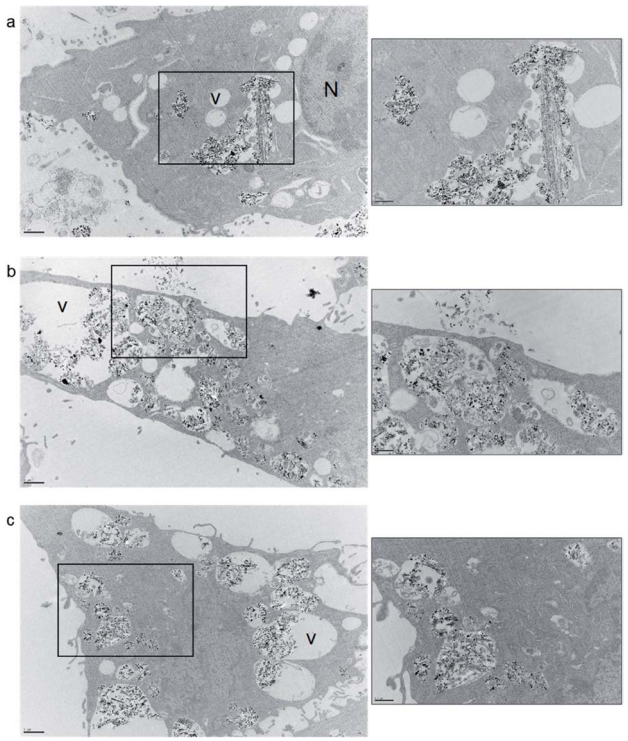

Fig. 5 Biological transmission electronic microscopy images illustrating cellular internalization of pSiNRs@SPIONs (a), pSiNRs@SPIONs-BIOT-NFL (b), or pSiNRs@SPIONs-FAM-NFL (c) in rat glioblastoma cells. F98 cells were incubated 72 hours at 37 °C with nanoparticles at 200 μg mL^{-1}. Images were taken with a TEM. Scale bars: 1 μm (left images) and 0.5 μm (right images). N for nucleus and V for vacuoles.

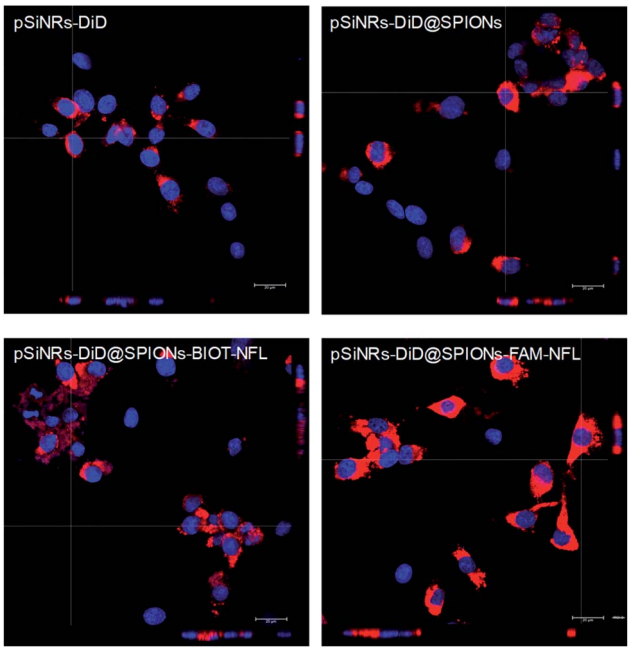

Fig. 6 Confocal experiments show cellular uptake of pSiNRs alone or functionalized with SPIONs, and with the NFL-peptide (BIOT or FAM) in rat glioblastoma cells. F98 cells were incubated 24 hours at 37 °C with nanoparticles at 10 μg mL^{-1}. Images were taken with a confocal microscope, nanoparticles loaded with DiD were visualized in red, and nucleus in blue. Pictures illustrating the orthogonal projections of cells treated. Experiments were performed at least triplicate. Scale bars: 20 μm.

observed with confocal microscope. Orthogonal projections presented in Fig. S36 in ESI† showed an important DiD fluorescence when F98 cells were treated with LNC-DiD demonstrating that DiD was internalized in GBM cells. Then, cells were treated with SPIONs added to LNC-DiD (LNC-DiD-SPIONs), weaker DiD fluorescence was observed, and no green-shift in fluorescence was detectable. Therefore, the combination of DiD and SPIONs is not able to create green fluorescence. Concerning the intensive green fluorescence under confocal microscope imaging from the multifunctional nanoparticles, we assume a possible Förster resonance energy transfer (FRET)[50] between the components (pSiNRs, SPIONs and DiD). In fact, porous silicon is well known to absorb the light and transfer the energy to the dye.[22]

Conclusions

In summary, a novel 3D shape-controlled nanostructure of porous silicon nanoparticles has been elaborated and applied to GBM cells treatment. Particles have been turned into powerful multifunctional nanosystems bearing magnetic guidance, fluorescent tracking and CPP in order to increase the treatment efficiency. The physico-chemical properties of the synthesized nanoparticles were fully characterized *via* complementary techniques in order to confirm the entire modifications. Furthermore, these nanoplatforms were efficient for *in vitro* studies onto human GBM cells. Overall, mitochondrial activity effects were demonstrated in particular with the targeted nanoparticles. The obtained results are promising for the improvement of GBM therapy, and the work is in progress to further extend the research on *in vivo* treatment.

Author contributions

A. C. synthesized and characterized the nanoparticles formulations. A. G. performed and analyzed *in vitro* experiments. G. G. and J. E. conceived the idea and led the project. A. C., and A. G., prepared the manuscript, and all authors contributed to the final version.

Conflicts of interest

The authors declare that they have no conflict of interest, with respect to the research, authorship, and/or publication of this article.

Acknowledgements

This project has been supported by 'Plan Cancer Inserm'. The authors gratefully thank to Daniela Neacsa for the XRD measurements, Carine Maaliki for the TGA measurements, Rodolphe Perrot from SCIAM (Service Commun d'Imageries et d'Analyses Microscopiques, Angers) for the confocal imaging, and Florence Manero from SCIAM for electron microscopy.

Notes and references

1 E. C. Holland, *Proc. Natl. Acad. Sci. U. S. A.*, 2000, **97**, 6242–6244.
2 R. Stupp, W. P. Mason, M. J. van den Bent, M. Weller, B. Fisher, M. J. B. Taphoorn, K. Belanger, A. A. Brandes, C. Marosi, U. Bogdahn, J. Curschmann, R. C. Janzer, S. K. Ludwin, T. Gorlia, A. Allgeier, D. Lacombe, J. G. Cairncross, E. Eisenhauer and R. O. Mirimanoff, *N. Engl. J. Med.*, 2005, **352**, 987–996.
3 Q. T. Ostrom, H. Gittleman, J. Xu, C. Kromer, Y. Wolinsky, C. Kruchko and J. S. Barnholtz-Sloan, *Neuro-Oncology*, 2016, **18**, v1–v75.
4 S. Bao, Q. Wu, R. E. McLendon, Y. Hao, Q. Shi, A. B. Hjelmeland, M. W. Dewhirst, D. D. Bigner and J. N. Rich, *Nature*, 2006, **444**, 756–760.
5 B. Y. S. Kim, J. T. Rutka and W. C. W. Chan, *N. Engl. J. Med.*, 2010, **363**, 2434–2443.
6 L. Battaglia, M. Gallarate, E. Peira, D. Chirio, E. Muntoni, E. Biasibetti, M. T. Capucchio, A. Valazza, P. P. Panciani, M. Lanotte, D. Schiffer, L. Annovazzi, V. Caldera, M. Mellai and C. Riganti, *J. Pharm. Sci.*, 2014, **103**, 2157–2165.
7 R. Karim, E. Lepeltier, L. Esnault, P. Pigeon, L. Lemaire, C. Lépinoux-Chambaud, N. Clere, G. Jaouen, J. Eyer, G. Piel and C. Passirani, *Nanoscale*, 2018, **10**, 13485–13501.
8 J. Zhou, T. R. Patel, R. W. Sirianni, G. Strohbehn, M.-Q. Zheng, N. Duong, T. Schafbauer, A. J. Huttner, Y. Huang, R. E. Carson, Y. Zhang, D. J. Sullivan,

J. M. Piepmeier and W. M. Saltzman, *Proc. Natl. Acad. Sci. U. S. A.*, 2013, **110**, 11751–11756.
9 H. Guerrero-Cázares, S. Y. Tzeng, N. P. Young, A. O. Abutaleb, A. Quiñones-Hinojosa and J. J. Green, *ACS Nano*, 2014, **8**, 5141–5153.
10 Z.-Y. Li, Y. Liu, X.-Q. Wang, L.-H. Liu, J.-J. Hu, G.-F. Luo, W.-H. Chen, L. Rong and X.-Z. Zhang, *ACS Appl. Mater. Interfaces*, 2013, **5**, 7995–8001.
11 J. Mo, L. He, B. Ma and T. Chen, *ACS Appl. Mater. Interfaces*, 2016, **8**, 6811–6825.
12 A. Pandey, S. Kulkarni, A. P. Vincent, S. H. Nannuri, S. D. George and S. Mutalik, *Int. J. Pharm.*, 2020, **588**, 119735.
13 A. Sharma, A. Kumar, C. Li, P. Panwar Hazari, S. D. Mahajan, R. Aalinkeel, R. K. Sharma and M. T. Swihart, *J. Mater. Chem. B*, 2021, **9**, 2505–2514.
14 J.-H. Park, L. Gu, G. von Maltzahn, E. Ruoslahti, S. N. Bhatia and M. J. Sailor, *Nat. Mater.*, 2009, **8**, 331–336.
15 E. Anglin, L. Cheng, W. Freeman and M. Sailor, *Adv. Drug Delivery Rev.*, 2008, **60**, 1266–1277.
16 A. Loni, L. T. Canham, T. Defforge and G. Gautier, *ECS J. Solid State Sci. Technol.*, 2015, **4**, P289–P292.
17 V. Lehmann, R. Stengl and A. Luigart, *J. Mater. Sci. Eng. B*, 2000, **69–70**, 11–22.
18 E. Nekovic, C. J. Storey, A. Kaplan, W. Theis and L. T. Canham, *ECS J. Solid State Sci. Technol.*, 2020, **9**, 024016.
19 J. Rytkönen, P. Arukuusk, W. Xu, K. Kurrikoff, Ü. Langel, V.-P. Lehto and A. Närvänen, *Mol. Pharmaceutics*, 2014, **11**, 382–390.
20 E. Secret, K. Smith, V. Dubljevic, E. Moore, P. Macardle, B. Delalat, M.-L. Rogers, T. G. Johns, J.-O. Durand, F. Cunin and N. H. Voelcker, *Adv. Healthcare Mater.*, 2013, **2**, 718–727.
21 B. Guan, A. Magenau, S. Ciampi, K. Gaus, P. J. Reece and J. J. Gooding, *Bioconjugate Chem.*, 2014, **25**, 1282–1289.
22 E. Secret, M. Maynadier, A. Gallud, A. Chaix, E. Bouffard, M. Gary-Bobo, N. Marcotte, O. Mongin, K. El Cheikh, V. Hugues, M. Auffan, C. Frochot, A. Morère, P. Maillard, M. Blanchard-Desce, M. J. Sailor, M. Garcia, J.-O. Durand and F. Cunin, *Adv. Mater.*, 2014, **26**, 7643–7648.
23 A. Chaix, K. El Cheikh, E. Bouffard, M. Maynadier, D. Aggad, V. Stojanovic, N. Knezevic, M. Garcia, P. Maillard, A. Morère, M. Gary-Bobo, L. Raehm, S. Richeter, J.-O. Durand and F. Cunin, *J. Mater. Chem. B*, 2016, **4**, 3639–3642.
24 O. Tabasi, C. Falamaki and Z. Khalaj, *Colloids Surf., B*, 2012, **98**, 18–25.
25 D. Nadarassan, A. Loni, L. T. Canham, N. Scoutaris, V. Trivedi and D. Douroumis, *Int. J. Pharm.*, 2021, **607**, 120840.
26 T. Tieu, M. Wojnilowicz, P. Huda, K. J. Thurecht, H. Thissen, N. H. Voelcker and A. Cifuentes-Rius, *Biomater. Sci.*, 2021, **9**, 133–147.
27 L. Gu, J.-H. Park, K. H. Duong, E. Ruoslahti and M. J. Sailor, *Small*, 2010, **6**, 2546–2552.
28 A. Bertucci, K.-H. Kim, J. Kang, J. M. Zuidema, S. H. Lee, E. J. Kwon, D. Kim, S. B. Howell, F. Ricci, E. Ruoslahti, H.-J. Jang and M. J. Sailor, *ACS Appl. Mater. Interfaces*, 2019, **11**, 23926–23937.
29 A. Chaix, E. Cueto-Diaz, A. Delalande, N. Knezevic, P. Midoux, J.-O. Durand, C. Pichon and F. Cunin, *RSC Adv.*, 2019, **9**, 31895–31899.
30 W. Y. Tong, M. Alnakhli, R. Bhardwaj, S. Apostolou, S. Sinha, C. Fraser, T. Kuchel, B. Kuss and N. H. Voelcker, *J. Nanobiotechnol.*, 2018, **16**, 38.
31 M. Luo, G. Lewik, J. C. Ratcliffe, C. H. J. Choi, E. Mäkilä, W. Y. Tong and N. H. Voelcker, *ACS Appl. Mater. Interfaces*, 2019, **11**, 33637–33649.
32 S. Sheykhzadeh, M. Luo, B. Peng, J. White, Y. Abdalla, T. Tang, E. Mäkilä, N. H. Voelcker and W. Y. Tong, *Sci. Rep.*, 2020, **10**, 2320.
33 R. H. Kang, J.-E. Jang, E. Huh, S. J. Kang, D.-R. Ahn, J. S. Kang, M. J. Sailor, S. G. Yeo, M. S. Oh, D. Kim and H. Y. Kim, *Nanoscale Horiz.*, 2020, **5**, 1213–1225.
34 A. Chaix, K. Rajoua, V. Stojanovic, K. El Cheikh, E. Bouffard, A. Brocéro, M. Garcia, M. Maynadier, A. Morère, M. Gary-Bobo, F. Favier, J.-O. Durand and F. Cunin, *ChemNanoMat*, 2018, **4**, 343–347.
35 T. Kim, G. B. Braun, Z. She, S. Hussain, E. Ruoslahti and M. J. Sailor, *ACS Appl. Mater. Interfaces*, 2016, **8**, 30449–30457.
36 H. A. Jeng and J. Swanson, *J. Environ. Sci. Health, Part A: Environ. Sci. Eng. Toxic Hazard. Subst. Control*, 2006, **41**, 2699–2711.
37 S. M. Hussain, K. L. Hess, J. M. Gearhart, K. T. Geiss and J. J. Schlager, *Toxicol. In Vitro*, 2005, **19**, 975–983.
38 N. Singh, G. J. S. Jenkins, R. Asadi and S. H. Doak, *Nano Rev.*, 2010, **1**, 5358.
39 H. Xie, Y. Zhu, W. Jiang, Q. Zhou, H. Yang, N. Gu, Y. Zhang, H. Xu, H. Xu and X. Yang, *Biomaterials*, 2011, **32**, 495–502.
40 D.-F. Liu, C. Qian, Y.-L. An, D. Chang, S.-H. Ju and G.-J. Teng, *Nanoscale*, 2014, **6**, 15161–15167.
41 R. Berges, J. Balzeau, A. C. Peterson and J. Eyer, *Mol. Ther.*, 2012, **20**, 1367–1377.
42 A. Griveau, C. Lepinoux-Chambaud and J. Eyer, *Int. J. Pharm.*, 2021, **605**, 120811.
43 D. Carradori, P. Saulnier, V. Préat, A. des Rieux and J. Eyer, *J. Controlled Release*, 2016, **238**, 253–262.
44 Y. Laurin, P. Savarin, C. H. Robert, M. Takahashi, J. Eyer, C. Prevost and S. Sacquin-Mora, *Biochemistry*, 2015, **54**, 3660–3669.
45 Z. Huang, N. Geyer, P. Werner, J. de Boor and U. Gösele, *Adv. Mater.*, 2011, **23**, 285–308.
46 H. Alhmoud, D. Brodoceanu, R. Elnathan, T. Kraus and N. H. Voelcker, *Prog. Mater. Sci.*, 2021, **116**, 100636.
47 Z. Qin, J. Joo, L. Gu and M. J. Sailor, *Prog. Mater. Sci.*, 2014, **31**, 252–256.
48 T. Nissinen, T. Ikonen, M. Lama, J. Riikonen and V.-P. Lehto, *Powder Technol.*, 2016, **288**, 360–365.
49 B. Bhattacharyya, D. Panda, S. Gupta and M. Banerjee, *Med. Res. Rev.*, 2008, **28**, 155–183.
50 D. M. Charron and G. Zheng, *Nano Today*, 2018, **18**, 124–136.